This article was published as
Materials Science & Engineering C 118 (2021) 111476
DOI: https://doi.org/10.1016/j.msec.2020.111476

***In vivo* time-course biocompatibility assessment of biomagnetic nanoparticles-based biomaterials for tissue engineering applications**

Fernando Campos [1,5], Ana Belén Bonhome-Espinosa[3], Ramón Carmona[4], Juan de Dios García López-Durán[3,5], Pavel Kuzhir[6], Miguel Alaminos[1,5], Modesto Torcuato López-López [3,5*], Ismael Angel Rodriguez [1,2,a*], Víctor Carriel [1,5,a]

[1]-*Department of Histology, Tissue Engineering Group, Faculty of Medicine, University of Granada, Granada, Spain*

[2]-*Department of Histology, Faculty of Dentistry, Nacional University of Cordoba, Cordoba, Argentina.*

[3]-*Department of Applied Physics, University of Granada, Avenida de la Fuente Nueva, 18071 Granada, Spain.*

[4]-*Department of Cell Biology, Faculty of Sciences, University of Granada, Campus Fuentenueva s/n, Granada, Spain.*

[5]-*Instituto de Investigación Biosanitaria ibs.GRANADA, Granada, Spain.*

[6]-*Laboratory of Physics, Matière Condensée, CNRS UMR 6622, University of Nice, Parc Valrose, 06108, Nice, Cedex2, France.*

[a] *These authors contributed equally: Victor Carriel, Ismael Angel Rodriguez.*

[*] *Corresponding: Prof. Dr. Modesto Torcuato López-López & Prof. Dr. Ismael Rodriguez, Department of Applied Physics and Department of Histology, Tissue Engineering Group, University of Granada, Granada, Spain. Email: modesto@ugr.es; ismaelrodriguez18@hotmail.com*

Abstract:

Novel artificial tissues with potential usefulness in local-based therapies have been generated by tissue engineering using magnetic-responsive nanoparticles (MNPs). In this study, we performed a comprehensive *in vivo* characterization of bio-engineered magnetic fibrin-agarose tissue-like biomaterials. First, *in vitro* analyses were performed and the cytocompatibility of MNPs was demonstrated. Then, bioartificial tissues were generated and subcutaneously implanted in Wistar rats and their biodistribution, biocompatibility and functionality were analyzed at the morphological, histological, hematological and biochemical levels as compared to injected MNPs. Magnetic Resonance Image (MRI), histology and magnetometry confirmed the presence of MNPs restricted to the grafting area after 12 weeks. Histologically, we found a local initial inflammatory response that decreased with time. Structural, ultrastructural, hematological and biochemical analyses of vital organs showed absence of damage or failure. This study demonstrated that the novel magnetic tissue-like biomaterials with improved biomechanical properties fulfill the biosafety and biocompatibility requirements for future clinical use and support the use of these biomaterials as an alternative delivery route for magnetic nanoparticles.

Key words: Tissue Engineering, Magnetic nanoparticles, Biomaterials, Bio-distribution, *In vivo* biocompatibility

1. Introduction

During the last years, magnetic nanoparticles (MNPs) have been evaluated in biomedicine for hyperthermia induction [1], cell labeling and separation [2], DNA separation [3], magnetic resonance imaging [4] and for drug or gene therapies [5], [6]. Iron oxides MNPs are the most commonly used, especially Fe_3O_4 (magnetite) and $_{\gamma}Fe_2O_3$ (maghemite), because these are stable from a thermal, chemical and colloidal standpoint. In addition, based on the MNPs magnetic properties, it was hypothesized that these particles could be guided to specific *in vivo* locations using a magnetic field gradient. This could be useful as an alternative method to concentrate growth factors, drugs or cells associated to the particles [7], [8], [9], and it has been postulated that MNPs could be useful tools for theracnostic [10] and tissue engineering applications as a tool for local-based therapies [11], [12], [13], [14] [15]. MNPs were previously tested for the generation of bioengineered magnetic tissue-like substitutes with improved properties, without affecting cell adhesion, proliferation, viability or differentiation *in vitro* [16], [17], showing a significant improvement of the biomechanical properties of these biomaterials [11], [17].

Concerning *in vivo* biodistribution of MNPs, it is clear that the administration route will be a critical factor determining bioavailability and *in vivo* functionality of MNPs [10]. To date, several studied focused on determining the fate of these particles when injected into the bloodstream [10], and results demonstrated that injected MNPs have a short lifespan, tend to accumulate in different organs and may have certain degree of cytotoxic effects [10, 18]. However, the *in vivo* biodistribution when particles are applied immersed within a biomaterial needs further characterization [12], and *in vivo* studies evaluating the cellular and molecular processes related to biocompatibility, biodegradability and bio-distribution of implanted magnetic hydrogels are in need. Our group previously developed a fibrin-agarose hydrogel (FAH), which was successfully used in numerous tissue engineering applications [19], [20], [21], [22], [23], [24], [25] [26] and is currently used in clinical trials with the approval of the Spanish Agency of Medicines and Medical Devices (AEMPS) according to the EU guidelines for clinical use [27]. Therefore, FAH can be an useful carrier candidate to be combined with MNPs in order to generate novel biocompatible magnetic tissue-like biomaterials [11], [17], [13].

The aim of this study was to determine the biocompatibility of FAH-based magnetic tissue-like biomaterials containing MagNP-OH magnetic nanoparticles and to study their *in vivo* biodistribution in a rat model. First, the structure and biocompatibility of magnetic hydrogels was determined *in vitro*. Then, magnetic scaffolds and scaffold-free MNPs were subcutaneously grafted and the host response was evaluated by magnetic resonance imaging, laboratory testing, histology and magnetometry after 12 weeks *in vivo*.

2. Materials and methods

2.1 *In vitro* analyses

2.1.1 Magnetic nanoparticles (MNPs) characterization

In this study, we used commercially available MNPs (Nanomyp, Granada, Spain) referred as MagNP-OH. These MNPs have a mean hydrodynamic diameter of 100-120 nm and are composed by a polycrystalline of magnetite core coated by methyl methacrylate-co-hydroxyl ethyl methacrylate-co-ethylene glycol dimethacrylate (MMA-co-HEMA-co-EGDMA). The MagNP-OH particles were prepared for analyses following previously described procedures [11], [17].

The ultrastructure and dimension of the MagNP-OH were determined by using a LIBRA 120 PLUS Carl Zeiss transmission electron microscope (TEM). In addition, the magnetic properties of the MagNP-OH were characterized by vibrating sample magnetometer VSM 4500 (EG&G Princeton Applied Research, USA).

2.1.2 Analysis of biocompatibility of the MagNP-OH on 2D cell cultures

2.1.2.1 Cell culture and cell-MagNP-OH interaction model

Human fibroblast primary cultures obtained from human oral mucosa biopsies were cultured in 24-well plates (2x104 cells/well) with Dulbecco's Modified Eagle Medium (DMEM) with 10 % Fetal Bovine Serum (FBS) and antibiotics/antimycotics commercial cocktail solution (all from Sigma-Aldrich, Germany) at 37°C and 5% CO2 during 24 h. MagNP-OH particles were added to cultured cells at a concentration of 0.5% and 1% (w/v) in DMEM (without FBS and antibiotics) and were kept in culture for 24 h, and biocompatibility was determined after this time. As positive controls of live cells (100% cell viability), the same cells were cultured without MagNP-OH particles. As negative controls (100% cytotoxicity), cells were incubated in the same medium with 1% of Triton X-100. Biocompatibility was analyzed in six independent samples and viability was evaluated 4 times in each sample (24 measures by condition and test).

2.1.2.2 In vitro assessment of MagNP-OH cytocompatibility

Cytocompatibility was evaluated using a combination of morphological analyses, functional WST-1 cell viability/proliferation assay and quantification of free DNA released from dead cells (able to detect cell membrane structural integrity), as previously described [20], [28], [29]. First, the morphological changes associated to the presence of MagNP-OH were determined by phase contrast microscopy. Then, we analyzed the metabolic activity of the human cells using commercially available WST-1 assays (Roche Diagnostic, Mannheim, Germany) using a Microplate Reader (Biochrom® Asys UVM340) at a wavelength of 450–690 nm [20], [28]. Finally, the DNA-released as a consequence of irreversible cell membrane damage was quantified by using a NanoDrop 2000 UV-vis spectrophotometer (Thermo Fisher Scientific) [12], [20].

2.1.2.3 Preparation of the magnetic tissue-like biomaterials

In this study, we prepared three types of scaffolds: non-magnetic FAH, and two types of magnetic FAH: FAH containing MagNP-OH (FAH-MNPs), and FAH containing MagNP-OH with the application of a definite magnetic field during gelation (FAH-MNPs-F). For the preparation of FAH and the magnetic scaffolds (FAH-MNPs and FAH-MNPs-F), we used a variation of a previously described method for non-magnetic FAH [19], [22], [28], [30], [31]. Briefly, hydrogels were generated by mixing 70% of human plasma, 13.5% of PBS phosphate buffer (0.1M, pH 7.2-7.4) containing or not MagNP-OH (0.5% v/v of final hydrogel volume) and 1.5% of tranexamic acid. This solution was carefully mixed and then, a 2% solution of $CaCl_2$ was added (10% of the final volume) to promote fibrin gelation, followed by a 5% volume of melted 2% type VII agarose in PBS. This mixture was aliquoted and kept in a cell incubator using standard culture conditions until complete gelation [11]. In the case of FAH-MNPs-F, the mixture was subjected to a vertical magnetic field (48 kA/m) during the first 5 minutes of the process of jellification in order to obtain an anisotropic biomaterial composed by aligned fibers as previously reported [11].

2.1.2.4 Analysis of biomechanical properties of the magnetic tissue-like biomaterials

Magnetic and non-magnetic tissue-like biomaterials were subjected to oscillatory shear strains of increasing amplitude and fixed frequency (1 Hz) and the corresponding oscillatory shear stress was assessed using a Haake MARS III (Thermo Fisher Scientific, Waltham, MA, USA) controlled stress rheometer at 37°C. The measuring system geometry was a 3.5 cm diameter parallel plate set with rough surfaces to avoid wall slip, and the rotating plate was adjusted to a normal force of 5 N. Measurements were conducted under oscillatory shear strains and the biomechanical properties of the different tissue-like biomaterials were studied by determining the complex viscoelastic modulus of each sample.

2.2 *In vivo* analyses

2.2.1 Laboratory animals

In this study, a total of eighty-five 12 week-old adult male Wistar rats weighing 250–300 g were used. Animals were maintained in the Experimental Unit of the University Hospital Virgen de las Nieves in Granada (Spain). Animals were housed in a temperature-controlled room (21 ± 1°C) on a 12 h light/dark cycle with *ad libitum* access to tap water and standard rat chow. These studies were performed according to the European Union and Spanish Government guidelines for the ethical care of animals (EU Directive No. 63/2010, RD 53/2013) and this project was approved by the CEEA ethical committee for animal experimentation (approval number: 03-7-15-311).

2.2.2 Surgical procedure and experimental groups

For the *in vivo* biocompatibility evaluation of magnetic tissue-like biomaterials, and to study the biodistribution of the MagNP-OH, animals were deeply anaesthetized by intraperitoneal injection of a mixture of acepromizine (Calmo-Neosan®, 0.001 mg/g of weight of the animal) and ketamine (Imalgene 1000®, 0.15 mg/g of weight of the animal). Each animal was randomly assigned to one of the following experimental groups (n=20 in each except for the control group):

- (i) FAH group: once anesthetized, a 1cm-long incision of was made in the forearm skin of each animal, a FAH tissue-like substitute was subcutaneously grafted, and the injury was repaired using absorbable sutures. These animals were used as a control group (no MNPs).
- (ii) FAH-MNPs group: in these animals, FAH containing 0.5% (v/v) MagNP-OH were implanted following the same procedure described for the FAH group.
- (iii) FAH-MNPs-F group: FAH containing 0.5% (v/v) MagNP-OH subjected to magnetic field during gelation were implanted.
- (iv) MNPs-INJ group: in this case, MNPs were implanted in the same area of groups i, ii and iii (forearm subcutaneous tissue), but particles were injected in this case. With this purpose, a subcutaneous injection of MNPs was given in both forearms of each rat (250 µl of a sterile physiological solution containing 12.5 mg of MagNP-OH).
- (v) CTR group: five healthy animals were used as controls.

Animals were euthanized after 1, 3, 5 or 12 weeks (n= 5 in each) by using an overdose of anesthetics followed by intracardiac perfusion of fixative.

2.2.3 Magnetic resonance imaging (MRI)

Magnetic Resonance Image (MRI) analysis was used to identify the grafted materials in each animal and to assess the effects of these materials on the morphology of some major body organs. For this purpose, 3 animals corresponding to each group (CTR, FAH, FAH-MNPs, FAH-MNPs-F and MNPs-INJ) were analyzed 12 weeks after the surgical procedure using a Biospec TM 70/20 USR device equipped with 7 Tesla Ultrashield Refrigerated magnets (Bruker, Germany). First, animals were anesthetized using isoflurane anesthetics and immobilized in a cradle designed for the analysis of laboratory rats. Then, a whole-body scan was performed on each animal, and the morphology of liver, kidneys, lymph nodes and spleen was evaluated. Then, the grafting site was specifically analyzed to determine the MRI morphology of the implant site and possible migration of the particles to local and regional tissues.

2.2.3 Hematological and biochemical studies

1.5 mL of blood were collected from 5 animals corresponding to 1, 3, 5 and 12 weeks of *in vivo* follow-up. Blood was stored in Eppendorf tubes containing 5% heparin. For complete blood count, a Sysmex KX-21N automatic analyzer (Roche, Florida, USA) was used as recently described [32], to determine the following hematological parameters: concentration of hemoglobin (HGB), erythrocytes count (RCB), hematocrit count (HCT), platelets (PLT), white blood cells (WBC), lymphocytes (LYM), neutrophils (NEUT), monocytes-basophils-eosinophils (MXD).

For biochemical tests, blood was centrifuged for 15 min at 3,500 rpm and the supernatant serum was collected for analysis using a clinical chemistry analyzer Cobas c311 (Roche Laboratories, Florida, USA). The following biochemical parameters were analyzed in each sample: Alanine aminotransferase (ALT), urea (UREA), creatinine (CREJ2), iron (IRON2) (all RTU kits from Roche Laboratories) [32].

2.2.4 Histological and histochemical studies

For the histological analyses, animals were deeply anesthetized and perfused with 4% neutral buffered paraformaldehyde. For all animals included in the study, the area of the implant (FAH, FAH-MNPs, FAH-MNPs-F and MNPs-INJ) was carefully dissected and postfixed in 4% neutral buffered formaldehyde for 24 h, dehydrated and embedded in paraffin. For animals corresponding to 1 and 12 weeks of follow-up, four vital organs (liver, kidneys, lymph nodes and spleen) were also extracted, postfixed and embedded in paraffin. Tissue blocks were sectioned at 5 μm of thickness, rehydrated and stained with hematoxylin-eosin (H&E) for histological evaluation. In addition, different histochemical techniques were used to determine tissue-specific normal parameters. The periodic acid-Schiff histochemical method (PAS) was used to evaluate the glycogen content of the liver, the glomerular basement membrane of the kidney and the basement membranes of each tissue and organ. To identify the presence of ferric iron, all tissues and organs were stained with Perls (Prussian blue reaction) histochemical method contrasted with H&E as described previously [12].

The percentage of positive area for Perls-positive histochemical reaction in the spleen was determined with ImageJ software (National Institutes of Health, USA) from each group at 1 and 12 weeks following a previously described methodology [28, 33].

2.2.5 Ultrastructural analyses

For the ultrastructural analyses, tissue samples corresponding to the 12 weeks follow-up period were obtained from each animal included in the *in vivo* study at the moment of the euthanasia. Samples were fixed in 2.5% glutaraldehyde, washed three times in cacodylate buffer and post-fixed in 1% osmium tetroxide. Tissues were then dehydrated and embedded in Epoxy resin, and sectioned. Ultrathin sections were stained with aqueous uranyl acetate and lead citrate, mounted on grids and analyzed in a Carl Zeiss EM902 transmission electron microscope (Carl Zeiss Meditec, Inc., Oberkochen, Germany). The presence of iron atoms in tissues was identified by Electron Energy-Loss Spectroscopy (EELS).

2.2.6 Magnetometry

After the euthanasia, we tracked the presence of particles at the site of implantation and vital organs. We checked the magnetic response of the samples with a neodymium magnet in a magnetic field gradient of 10 mT/mm and a maximum field of 470 mT. In addition, we quantified the magnetic response of the samples by means of magnetometry measurements using a vibrating sample magnetometer VSM 4500 (EG&G Princeton Applied Research, USA) at room temperature. For this, similar volumes of tissue (equivalent to 50 mg of mass) were used from each condition. The detection limit of the magnetometer was 0.001 emu/g, which corresponds to approximately 30 μg of particles. These analyses were performed in animals corresponding to 12 weeks of *in vivo* follow-up.

2.2.7 Statistical analyses

In this study, all variables were subjected to Shapiro-Wilk test of normality and resulted to be non-normally distributed. Therefore, Fisher Exact Test and Mann-Whitney *U* test were used to determine statistical differences between comparison groups. All variables were analyzed by using the software SPSS 16.00 and results were shown as mean ± standard deviation (SD). In this study, $p<0.05$ was considered as statistically significant in two-tailed tests.

3. Results and Discussion

3.1 *In vitro characterization and biocompatibility*

First, our ultrastructural analysis of the MagNP-OH used in this study showed allowed us to confirm that the average diameter of these nanoparticles was 100-120 nm, size that is considerably higher than other single domain MNPs frequently used by other authors in tissue engineering (30-40 nm) [15], [16], [34], [35], [36], [37]. Interestingly, particles tended to form polycrystalline aggregates externally coated by a polymeric matrix surrounding each aggregate (Figure 1A). Magnetic characterization of the MagNP-OH revealed the typical soft ferromagnetic character of these MNPs, with negligible remnant magnetization, and a saturation magnetization of 161±7 kA/m (Figure 1B). It is well known that the size of the MNPs is directly related to the magnetic response of the particles, and multidomain MNPs (> 50 nm) commonly show higher magnetic response as compared to small particles [38]. Therefore, the polycrystalline aggregates generated in the present work may have the added value of having improved properties for use in tissue engineering [11], [17], [12].

Regarding *in vitro* cytocompatibility of human cells cultured in the presence of MagNP-OH, we carried out a combinate analysis at three levels: cell morphology, cell function and integrity of the cell membrane. Results show that, in general, these MNPs are highly cytocompatible. In the first place, co-culture of these MNPs with human cells was not able to modify the typical elongated spindle-like shape of viable human fibroblasts,

suggesting that these cells remained highly viable, and MNPs were mostly found homogeneously distributed in the extracellular space of the cells (Fig. 1C). In fact, morphology of these cells was comparable to positive control cells cultured without MNPs and very differernt to the small, rounded-shape appearance of negative control dead cells. To confirm these results at the functional level, we then analyzed the functionality of the cellular mitochondrial dehydrogenase by WST-1 assay. Results showed high levels of metabolic activity in cells containing MagNP-OH (at the concentration of 1% and 0.5%) with values comparable ($p>0.05$) to the positive control group. Positive controls and both experimental groups containing MagNP-OH showed significantly higher WST-1 values as compared to the negative control group ($p<0.0001$) (Figure 1D), suggesting high metabolic activity [20, 28]. Finally, viability was analized at the structural level by quantifying released DNA from cells cultivated in the presence of the MagNP-OH (Figure 1E), which is unfailingly associated to a cell membrane disruption [20, 28]. Results showed low cell mortality in positive controls and in both experimental groups (1% and 0.5%), with no differences between positive controls and cells cultured with MagNP-OH ($p>0.05$). However, mortality was significantly higher in negative controls ($p=0.0020$). These results are in agreement with the high cytocompatibility previously observed in hydrogels containing MagNP-OH [17], especially when these particles were coated with a polimer such as polyethylene glycol (PEG) [12]. The polymeric coating of MNPs provides hidrophilic properties that may improve stabilization in coloidal suspension and increase biocompatibility [10], [39]. Alltogether, these results support the high *in vitro* biocompatibility of the coated MagNP-OH used in this study.

Once the cytocompatibility of MagNP-OH was evaluated *in vitro*, we generated magnetic tissue-like biomaterials containing these particles. The rheological characterization of FAH-MNPs and FAH-MNPs-F revealed that incorporation of MagNP-OH considerably increased the strength of the tissue-like biomaterials as compared to control nonmagnetic FAH for the complex viscoelastic modulus $G^* = \left[\left(G'\right)^2 + \left(G''\right)^2\right]^{1/2}$ (Figure 1F), for both the biomaterials subjected to magnetic fields during the polymerization and materials devoid of these fields. These findings are in agreement with our previous studies showing that MNPs can considerably improve the biomechanical properties of FAH, thus increasing their putative usefulness in tissue engineering and regenerative medicine [11], [17], [12].

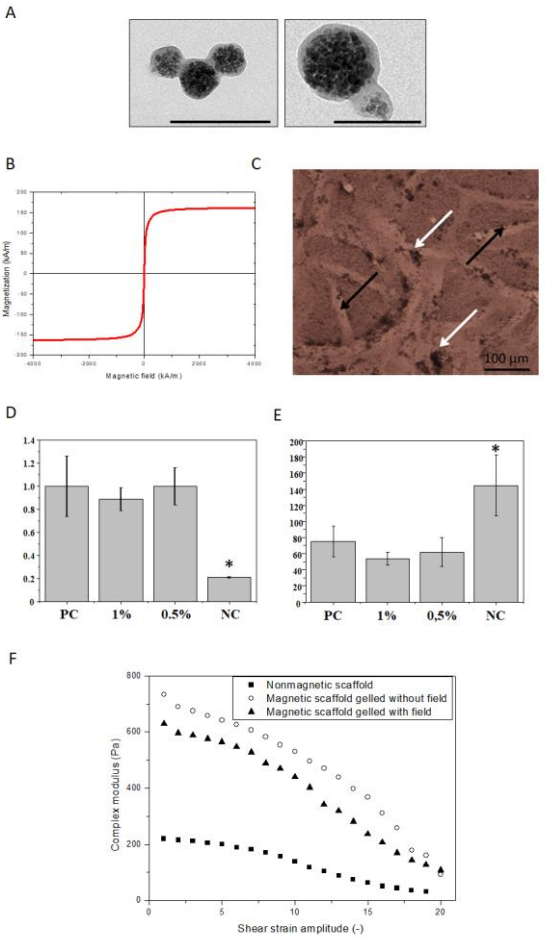

Figure 1. *In vitro* characterization of the MagNP-OH particles used in this study. A) Transmission electron microscopy ultrastructural analysis of MagNP-OH particles. Scale bar: 200 nm (left) and 100 nm (right). B) Magnetization curve of MagNP-OH particles. C) Phase contrast microscopy image of gingival human fibroblasts culturee with MagNP-OH particles. Cells are labeled with black arrows and MagNP-OH particles are highlighted with white arrows. D) Results of the cellular metabolic activity as determined by WST-1 assay. E) Analysis of cell membrane integrity as determined by DNA quantification. In D and E, values correspond to averages and standard deviations.* Results are statistically different to all the other study groups. PC: positive controls; NC: negative controls. F) Biomechanical properties are shown as the complex viscoelastic modulus of nonmagnetic FAH, FAH-MNPs and FAH-MNPs-F.

3.2 *In vivo evaluation*

An accurate monitoring and analysis of the fate of MNPs grafted *in vivo* in laboratory animals is essential for their future clinical translation and practical application [40]. Ideally, biocompatibility of grafted MNPs should be assessed by using a combination of invasive and non-invasive methods allowing a precise evaluation of the fate of the MNPs and the potential metabolic pathways and organs involved in MNPs metabolism and biodegradation. Consequently, animals grafted with the different materials used were subjected to an array of highly accurate evaluation methods that included MRI, magnetometry, hematological, biochemical and histological analyses in order to determine biocompatibility and the outcome of the grafted materials. In addition, analyses were performed at the local and the distal level as requested by most National Medicines Agencies for Advanced Therapies Medicinal Products [41]. In this sense, we first analyzed the local graft site in order to

determine *in situ* biosafety, temporal stability and migration to neighbor tissues. Then, we analyzed four key distal organs to shed light on the possible distal effects of the grafted biomaterials, including distal organ migration. In general, all these analyses allowed us to demonstrate that the biomaterials used in the present work are safe and comply with the main biosafety requirement for future clinical use.

In situ analysis of the implant site using MRI (Fig. 2) showed that non-magnetic FAH remained at the grafting site and were locally metabolized and reabsorbed in 12 weeks. In contrast, magnetic biomaterials containing MagNP-OH, as well as the injected MagNP-OH remained located in the implant site after 12 weeks of *in vivo* follow-up. These results coincide with the magnetometric analyses showing that controls and animals grafted with FAH were negative, whereas all animals with grafted MagNP-OH showed a highly positive magnetic response at the grafting site after 12 weeks of follow-up.

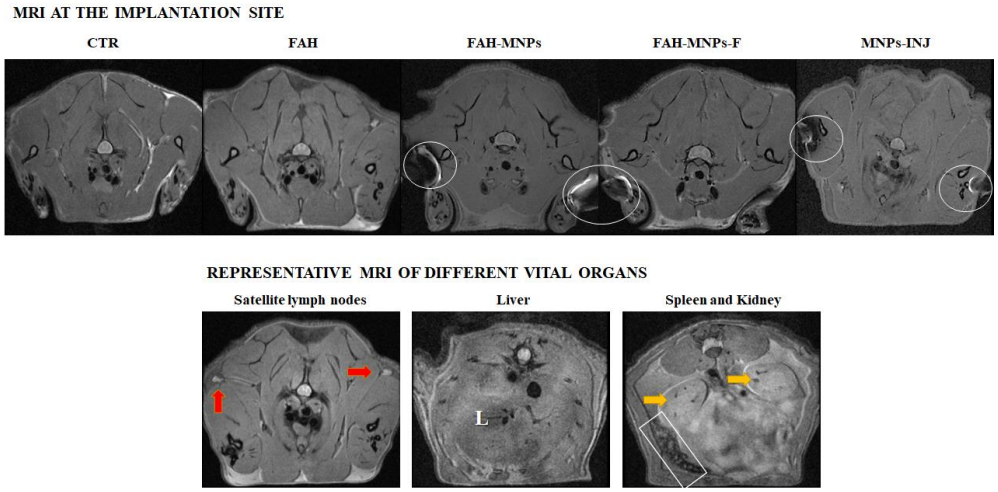

Figure 2. Magnetic Resonance Images (MRI) analysis of animals with the different materials grafted *in vivo* for 12 weeks. Images were taken at the grafting site (top panel) and distal organs (lower panel). Red arrows: satellite lymph nodes; yellow arrows: kidneys; L: liver; white circles: hyperintense areas corresponding to MagNP-OH accumulation at the implantation site; white rectangle: spleen. CTR: control animals; FAH: fibrin-agarose hydrogels; FAH-MNPs: FAH containing MagNP-OH; FAH-MNPs-F: FAH containing MagNP-OH subjected to magnetic field during gelation; MNPs-INJ: MNPs injected subcutaneously.

Then, the implantation site was analyzed histologically. In this regard, most animals showed an initial mild local inflammatory reaction restricted to the tissues surrounding the implanted materials, but no signs of necrosis, infection, rejection or malignization were found in any of the groups (Fig. 3). This reaction was similar in all groups grafted with biomaterials (FAH, FAH-MNPs and FAH-MNPs-F), and tended to decrease over the time. In FAH group, it was found that the number of inflammatory cells, especially macrophages, decreased with time and almost disappeared after 12 weeks. An interesting finding of our study was that the three groups in which MNPs were grafted tended to encapsulate the grafts, with the formation of a central Perls-positive nucleus surrounded by a connective tissue capsule. Although we found a single nucleus in the FAH-MNPs and FAH-MNPs-F groups, particles tended to form several independent nuclei in the MNPs-INJ group, at least during the first 5 weeks (Figure 3). These results confirm the absence of an increased inflammatory reaction driven by the MNPs implant and point out the usefulness of the FAH-MNPs model as a straightforward way of providing the host tissue with MNPs that could exert a positive clinical effect [42] [43]. As compared to injection, surgical

implantation of a tissue-like magnetic material allows a more efficient control of the grafting site and, according to our results, favor the MNPs containment and enhances encapsulation of the whole grafted mass in a single nucleus, thus preventing the connective tissue infiltration and grafts disaggregation or dispersion found in the MNPs-INJ group. In addition, the MNPs corresponding to the FAH-MNPs-F group showed a clear definite alignment and orientation of the MNPs during the first weeks, even though this orientation was lost after 5 weeks. Three-dimensional orientation of biomaterials is one of the goals of current tissue engineering, since most human tissues are characterized by a nonlinear and anisotropic mechanical behavior [44] due to the non-random distribution of its components, and this distribution is essential for its proper *in vivo* function. The use of FAH-MNPs-F could contribute to obtain MNPs-based bioartificial tissues with defined alignment with added value for use in regenerative medicine [45].

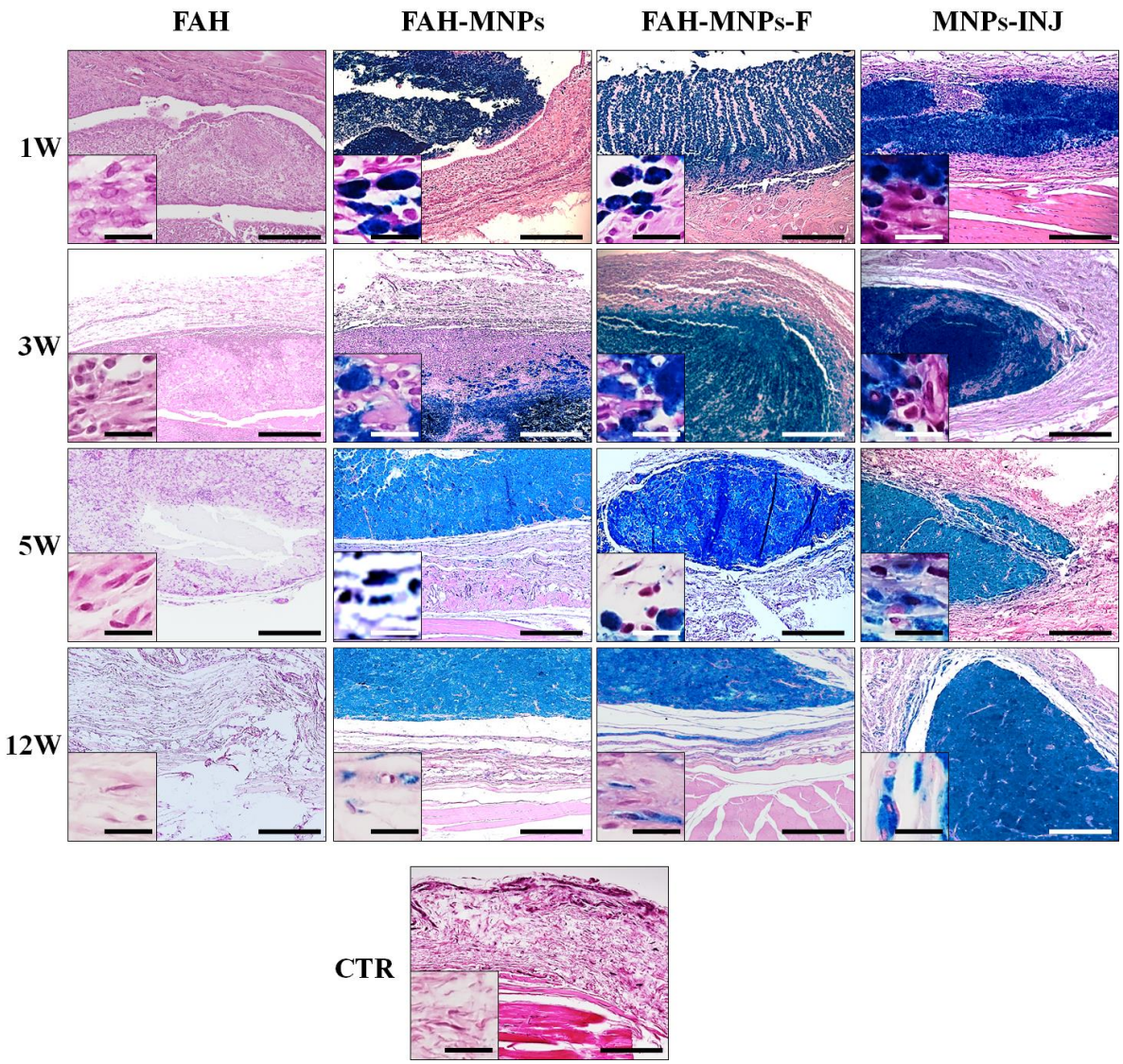

Figure 3. Perls histochemical results of grafted biomaterials and injected MNPs at 1, 3, 5 and 12 weeks *in vivo*. CTR: control animals; FAH: fibrin-agarose hydrogels; FAH-MNPs: FAH containing MagNP-OH; FAH-MNPs-F: FAH containing MagNP-OH subjected to magnetic field during gelation; MNPs-INJ: MNPs injected subcutaneously. Scale bars: 300µm (large images) and 20µm (inserts).

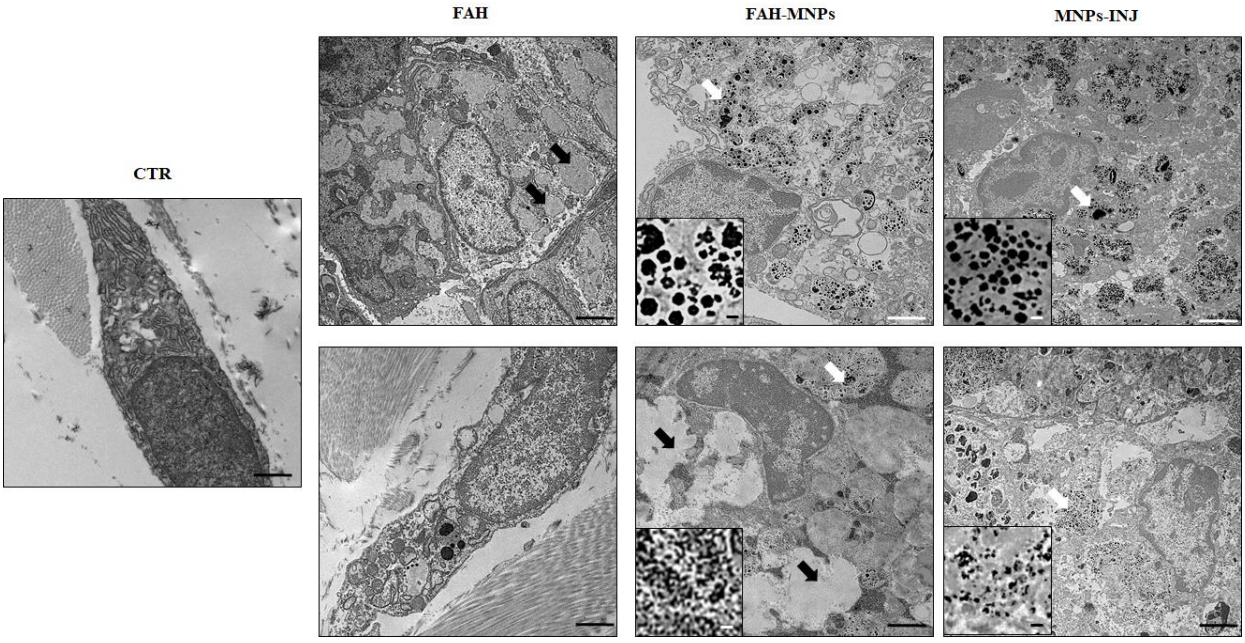

Figure 4. Representative images corresponding to the ultrastructural analysis of materials grafted *in vivo* for 12 weeks. CTR: control animals; FAH: fibrin-agarose hydrogels; FAH-MNPs: FAH containing MagNP-OH; MNPs-INJ: MNPs injected subcutaneously. Black arrow phagosome with agarose and white arrow MNPs. Scale bars: 300µm (large images) and 20µm (inserts).

Furthermore, we carried out TEM analyses to determine the biocompatibility of each biomaterial at the ultrastructural level after 12 weeks of the surgical procedure. On the one hand, host tissues corresponding to the FAH group showed macrophages with intracellular phagosomes containing rests of the biomaterial, along with extracellular matrix mainly consisting of collagen fibers similar to control tissues (Fig. 4). On the other hand, animals grafted with MNPs showed very similar behavior regardless of the specific group considered (FAH-MNPs, FAH-MNPs-F and MNPs-INJ). In all these groups, we found numerous host cells compatible with macrophages containing abundant intracellular MNPs that tended to keep their original polycrystalline aggregate pattern inside the cells. Most of the particles gathered in cytoplasmic vesicles that could correspond to endosomes or secondary lysosomes, as well as large phagosomes. MagNP-OH were also found in the extracellular space. No signs of necrosis or cell alterations were detected in any of the study groups. These findings confirm the high biocompatibility of the different materials used in this study. In agreement with previous reports, our results suggest that iron oxide nanoparticles are mostly engulfed within the human cells and do not cause any detectable alterations in these cells [10, 46]

Once the local implant site was analyzed, we evaluated the morphology, structure and function of several major distal organs of each animal to determine the possible distal effects of each biomaterial as part of the global biocompatibility and biosafety assessment required for future clinical use [41]. In this regard, the whole-body MRI scan analysis of each animal and the specific analysis of four key organs playing a role in metabolizing and processing a biomaterial grafted *in vivo* -liver, kidneys, lymph nodes and spleen- revealed a perfectly normal morphology devoid of detectable alterations (Fig. 2). No MNPs were detected by MRI in any of these organs. Similarly, analysis of the different organs using magnetometry revealed a negative signal in all animals after 12 weeks of *in vivo* follow-up. These results suggest that MagNP-OH stayed at the grafting site and did not tend to migrate, supporting again the excellent biocompatibility and stability of this type of MNPs.

At the histological level, the structural analysis of distal organs confirmed the absence of alterations during the whole study. Indeed, no signs of inflammation, fibrosis, necrosis or other detectable tissue alterations were observed in histological sections of liver, kidneys, lymph nodes and spleen stained with H&E in any of the groups (Supplementary Fig. S1). Similarly, PAS staining analysis (Supplementary Fig. S2) confirmed that the content of glycogen was normal in hepatocytes of all groups of animals, and the glomerular and non-glomerular basement membranes were also free from detectable alterations. These results are in agreement with previous studies demonstrating that this type of MNPs coated with different polymers can be safely used without significant histological alterations of vital organs [12], [47], whereas other types of particles were associated to histological lesions in liver and kidney [48].

In order to identify any possible particle migration to distal organs, we also analyzed these organs using the Perls histochemical technique, which is specific for detection of iron in cells and tissues. Results showed very few or no particles in liver and kidney at 1 and 12 weeks, but a positive reaction was found in spleen and lymph nodes at both analyzed times (Fig. 5). These findings are in agreement with previous reports demonstrating that nanoparticles of different nature tend to be massively captured by cells of the mononuclear phagocyte system [49]. Hence, we found that lymph nodes were Perls-negative in CTR and FAH group, whereas animals with grafted MNPs (FAH-MNPs, FAH-MNPs-F and MNPs-INJ) showed small Perls-positive areas after 1 week, and moderate to intense Perls-positive areas after 12 weeks, especially in the case of the injected MNPs. Then, we analyzed both components of the rat spleen (the red and the white pulp), and we found that the staining area and intensity was higher in this organ than in the rest of organs. As expected, the red pulp of the spleen was very positive to the Perls method in all groups, including controls, but this reaction became significantly more intense after 12 weeks in FAH-MNPs, FAH-MNPs-F and MNPs-INJ groups ($p<0.05$). These findings are consistent with the primary function of the red pulp, which is related to filtering peripheral blood from antigens, foreign bodies and all kinds of substances that may arrive to the blood, blood iron turnover, as well as serving as a huge reservoir of monocytes [18]. The white pulp, however, was mostly negative for this staining technique, although the marginal zone (in which antigen-presenting cells, such as dendritic cells and macrophages exists) was positive at 12 weeks in FAH-MNPs, FAH-MNPs-F and MNPs-INJ groups. Quantification of the Perls-positive areas in the red pulp (Figure 6) demonstrated no significant differences among samples at 1 week ($p>0.05$), but a significant increase was found at 12 weeks in the FAH-MNPs and MNPs-INJ groups ($p<0.05$). In fact, the three groups in which MNPs were grafted in animals, showed significant differences vs. control at week 12 ($p<0.05$). These results were corroborated at the ultrastructural level by TEM analysis confirming the presence of macrophages containing electrodense iron-rich granular material identified as iron by EELS in all experimental groups (Fig. 6). In contrast with the macrophages observed within grafted biomaterials, in spleen these cells contained iron-rich granular intracytoplasmic vesicles, but polycrystalline aggregates were not detected.

The presence of abundant cells containing iron in the spleen of all animal groups can be explained by the important role that the spleen plays in mechanical filtration of red blood cells and hemoglobin iron recycling and turnover [18]. The increase observed in animals in which MagNP-OH were grafted, strongly suggests that MNPS could progressively reach to the spleen through blood circulation, as other authors demonstrated by intraperitoneal injection of RITC-labeled MNPs [10], [50]. The fact that our magnetometry and MRI analyses were negative could probably be explained by the low concentration of MagNP-OH that reached the spleen, which was probably below than 30 μg, which is the minimum concentration required for detection by magnetometry and MRI. Another possibility is that MagNP-OH were progressively transformed into non-

magnetic iron forms by host cells as previously suggested [47]. Interestingly, previous works showed that superparamagnetic iron-oxide NPs show identical distribution pattern when administered *in vivo* [51].

In consequence, our histological results, in line with results published by other authors, highlight the relevance of the administration route and NPs size in the subsequent organic biodistribution [10], and confirm that MagNP-OH tend to remain stable at the implant site, with some particles biodistributed to lymphoid organs, without altering their histological structure and function.

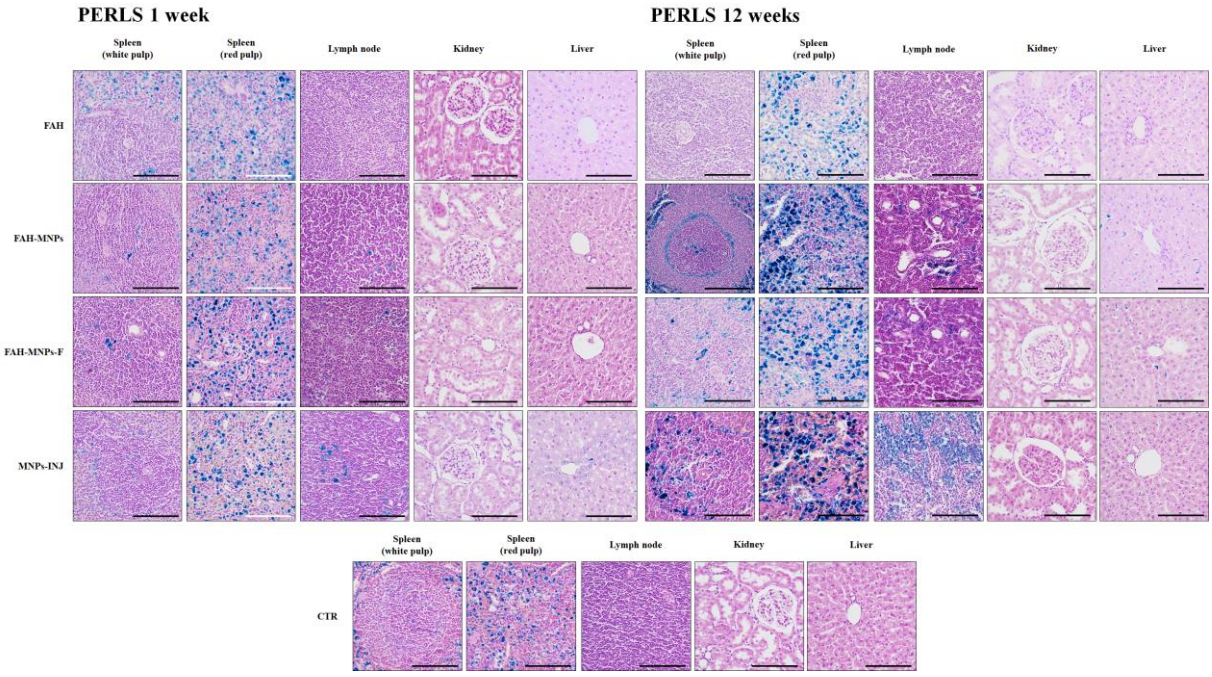

Figure 5. Perls histochemical results of distal organs at 1 and 12 weeks. FAH: fibrin-agarose hydrogels; FAH-MNPs: FAH containing MagNP-OH; FAH-MNPs-F: FAH containing MagNP-OH subjected to magnetic field during gelation; MNPs-INJ: MNPs injected subcutaneously; CTR: control animals. Scale bar 100 µm

PERLS-POSITIVE AREAS IN SPLEEN RED PULP	CTR	FAH	FAH-MNPs	FAH-MNPs-F	MNPs-INJ
1 week	3.28 ± 0.55	3.54 ± 0.75 (p=0.9990)	5.77 ± 0.61 (p=0.4977)	9.64 ± 1.38 (p=0.0818)	8.61 ± 0.72 (p=0.1338)
12 weeks	7.77 ± 0.89	5.43 ± 0.15 (p=0.5679)	22.84 ± 1.83 (p=0.0056)*	18.62 ± 1.81 (p=0.0370)*	28.25 ± 2.45 (p=0.0004)*
1 week vs. 12 weeks	(p=0.2134)	(p=0.9990)	(p=0.0010)*	(p=0.1070)	(p=0.0009)*

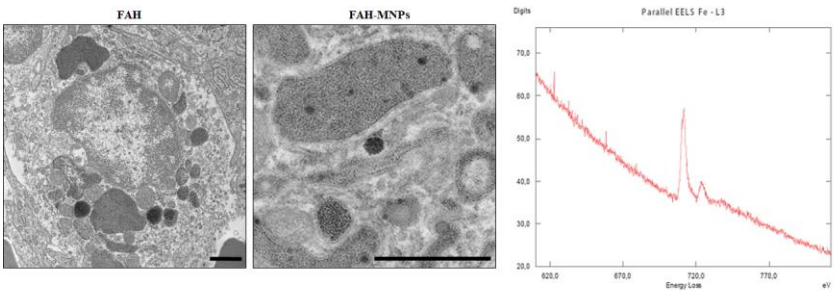

Figure 6. Quantitative results of Perls positive histochemical reaction and EELS in the red pulp of the spleen in each group and control. The table on top shows the results of the quantification of the percentage of

area corresponding to Perls-positive signal. The figures below show illustrative ultrastructural images of macrophages containing iron in intracellular phagosomes corresponding to two groups of animals (FAH and FAH-MNPs), along with an EELS spectrum with a peak corresponding to intracellular iron. CTR: control animals; FAH: fibrin-agarose hydrogels; FAH-MNPs: FAH containing MagNP-OH; FAH-MNPs-F: FAH containing MagNP-OH subjected to magnetic field during gelation; MNPs-INJ: MNPs injected subcutaneously. Values in the table are shown as mean ± standard deviation for each group of animals and each follow-up time, and the statistical p values corresponding to the comparison of these values with CTR are shown in brackets. In the last row, the statistical p values corresponding to the comparison of values at 1 week vs. values at 12 weeks are shown for each study group. Significant differences ($p<0.05$) are highlighted with asterisks (*). Scale bar for FAH = 1µm and scale bar for FAH-MNPs = 2µm

	HEMOGRAM								
	General count					WBC/White cells			
	WBC (10^3)	RBC (10^6)	HGB	HCT	PLT (10^5)	LYM	MXD	NEUT	
	μL^{-1}	μL^{-1}	g/dL	%	μL^{-1}	%	%	%	
FAH	3.04±1.51*	7.14±0.22*	13.5±0.52	39.54±1.1	5.16±1.99	45.68±23.56	32.56±22.96	21.76±4.64	1 W
	4.56±3.31	7.61±0.06	14.14±0.51	42.28±0.66	4.60±2.59	64.38±14.8	12.96±0.86	22.66±14.22	3 W
	2.75±0.26*	8.04±0.4	14.15±0.27	43.78±1.3	6.57±0.23	77.63±4.06	9.25±3.02	13.13±5.75	5 W
	9.74±3.89	8.15±0.38	14.32±0.2	44.06±1.93	5.11±3.63	68.5±16.18	9.32±3.65	22.18±13.58	12 W
FAH-MNPs	2.4±1.27	7.47±0.64	13.22±1.48	40.02±4.35	5.63±2.96	42.08±26.77	33.02±25.75	24.84±12.87	1 W
	5.18±3.11	7.51±0.3	14.16±0.76	42.26±2.17	3.82±2.16	62.02±15.52	13.34±2.57	24.64±16.25	3 W
	2.48±1.09	8.11±1.48*	14.18±9.93	44.27±1.72	6.24±2.57	72.7±16.81	5.92±1.78	21.08±9.9	5 W
	2.94±3.52	7.83±0.68	14.16±0.76	42.48±4.15	8.74±0.84	80.32±3.35*	15.28±4.59	2.56±5.96	12 W
FAH-MNPs-F	3.63±2.1	7.76±0.38	13.83±0.25	42.43±1.85	5.61±1.21	66.25±8.58	13.83±5.93	19.93±6.41	1 W
	2.46±0.46	7.62±0.44	13.58±0.39	41.18±1.69	6.31±0.72	76.02±3.35	11.04±1.35	12.94±2.11	3 W
	5.36±4.05	7.77±4.09*	13.91±0.6	42.73±1.81	3.62±2.48	68±12.91	16.02±7.07	15.98±6.97	5 W
	5.72±1.73	8.46±0.62*	14.52±0.6	45.66±3.1	3.78±4.1	69±13.41	12.64±2.97	18.36±11.6	12 W
MNPs-INJ	2.48±0.43	7.82±0.24	13.78±0.42	42.8±1.86	4.88±2.75	72.08±6.03	12.53±1.24	15.4±6.02	1 W
	1.92±0.64	7.54±0.26	13.5±0.24	41.22±1.51	6.26±0.73	73.2±7.71	14.92±5.72	11.88±2.58	3 W
	1.78±0.29	8.03±0.23*	14.08±0.83	43.94±2	5.94±2.82	74.5±3.71	10.82±4.98	14.68±6.67	5 W
	7.1±3.74	7.57±0.89	13.75±1.61	41.45±5.4	4.33±4.58	65.83±4.67	10.03±3.42	24.15±6.5	12 W
CTR	5.93±3.46	7.72±0.11	13.9±0.5	42.25±1.07	2.58±2.71	63.03±15.39	14.33±6.75	22.65±13.16	

Table 1. Hematological profile. Summary of the mean and SD of parameters evaluated at 1, 3, 5 and 12 week. White blood cells (WBC), erythrocytes count (RBC), concentration of hemoglobin (HGB), hematocrit count (HCT), platelets (PLT), lymphocytes (LYM), monocytes-basophils-eosinophils (MXD), neutrophils (NEUT). Significant differences ($p<0.05$) between experimental and control groups are highlighted with asterisks (*).

After the morphology and structure of local and distal tissues and organs were determined, we analyzed the effect of the different biomaterials on each animal group at the functional level. In this regard, hematological studies revealed that all parameters evaluated here were within the physiological range of normal values described in the literature for the Wistar rat (Table 1) [48]. However, some specific parameters showed significant differences with the control animals used in this study. In the case of the red blood cells (RBC), we observed a significant decrease of RBC counts in the FAH group at 1 week as compared to controls ($p=0.009$), which could be a consequence of the recent surgical procedure. In contrast, a significant increase of the number

of RBC was observed after 5 weeks in FAH-MNPs (p=0.016), FAH-MNPs-F (p=0.016) and MNPs-INJ (p=0.028), and also after 12 weeks for FAH-MNPs-F (p=0.028) as compared to controls. Interestingly, the increase of RBC values was not accompanied by significant variations of the concentration of hemoglobin (HGB) or hematocrit (HCT). The leukocytes (WBC) count showed a transient reduction in the FAH group at 5 weeks as compared to controls (p=0.009), although the leukocyte formula was normal for all the study groups except for an increase of lymphocytes (LYM) at 12 weeks in FAH-MNPs group (p=0.010). Finally, the evaluation of platelets (PLT) showed an increase in all experimental groups over the time as compared to control animals. All these variations, which fell into the normal parameters of healthy Wistar rats [48], could be related to the host adaptive physiological response to the surgical procedure, healing process, active hydrogel biodegradation and MagNP-OH phagocytosis, being these results in line with the histological findings. A similar result was found for the biochemical parameters analyzed in plasma of each animals, which were normal in most cases (Table 2). First, the levels of circulating iron were similar to control animals at all study times (p>0.05). The lack of increase of circulating free iron supports the idea that MNPs remained stable and were not able to release a significant amount of iron to the circulation. Similarly, most hepatic function-related parameters fell within the physiological range of this species, except for an initial transient decrease of ALT in MNPs-INJ (p=0.028) that normalized thereafter. Finally, the two biochemical markers of renal function (urea and creatinine) were normal in all study groups. Additionally, the renal function-related parameters urea and creatinine (CREJ2) showed a transitory increase over the time in all experimental groups as compared to controls, which tended to normalize with time.

Altogether, these hematological and biochemical results confirmed that the use of MagNP-OH is safe and *in vivo* implantation of these MNPs is not associated to a vital organ failure. Although some slight variations were found in specific groups of animals, values were in agreement with the physiological ranges described in the literature [48], and showed a clear normalization over the time. In addition, the normalization of blood and biochemical parameters is in line with the quantitative results observed in Wistar rats in which the sciatic nerve was repaired with acellular nerve grafts [32]. These findings confirm again that both administration routes for the MagNP-OH (injected or encapsulated) were safe for the host animal. In contrast, a previous study showed that the high-dose oral administration of other types of nanoparticles based on silver was related to hepatic and renal affection at the biochemical level, what clearly differed from our findings [48]. Finally, the hematological and biochemical profiles were in concordance with the histological and MRI results showing normal structure and morphology of distal organs, and. All this suggests that the *in vivo* injection and the subcutaneous implantation of the magnetic materials generated in this work was fully biocompatible and fulfilled the strict biosafety criteria required for future clinical use.

	BIOCHEMICAL				
	Liver	**Kidney**		**Other parameters**	
	ALT	CREJ2	UREA	Fe	
	U/L	mg/dl	mg/dl	µg/dl	
FAH	46.28±10.26	0.75±0.08	42.32±6.71	162.27±0.29	1 w
	40.44±7.38	0.65±0.14	43.28±7.34	170.25±0.33	3 w
	41.35±17.39	0.6±0.24	38.08±13.76	164.214±0.61	5 w
	53.54±16.03	0.6±0.08	36.94±2.65	181.191±0.22	12 w
FAH-MNPs	141±144.53	0.7±0.15	46.66±8.73	147.31±0.31	1 w

	79.2±65.15	0.72±0.08	43.84±5.97	187.51±0.32	3 w
	42.08±10.65	0.66±0.15	38.22±2.67	171.19±0.40	5 w
	74.68±60.94	0.54±0.11	35.08±4.48	249.36±1.91	12 w
FAH-MNPs-F	45.75±6.72	0.84±0.18	37.5±8.76	157.85±0.42	1 w
	46.82±11.49	0.69±0.1	41.5±4.6	160.15±0.15	3 w
	46.61±26.92	0.53±0.05	39.59±4.93	172.2±0.27	5 w
	45.28±9.17	0.66±0.05	38.72±5.84	148.91±0.10	12 w
MNPs-INJ	30.2±7.83*	0.65±0.11	39.3±7.57	155.15±0.25	1 w
	35.94±6.19	0.53±0.08	38.98±4.74	183.92±0.22	3 w
	62.86±30.07	0.71±0.11	38.56±4.89	168.49±0.26	5 w
	44.62±10.09	0.74±0.11	39.58±5.2	164.91±0.29	12 w
CTR	39.55±5.55	0.46±0.14	34±2.81	184.36±0.23	

Table 2. Biochemical profile. Summary of the mean and SD of parameters evaluated at 1, 3, 5 and 12 week. Alanine aminotransferase (ALT), urea (UREA), creatinine (CREJ2) and iron (Fe). Significant differences ($p<0.05$) between experimental and control groups are highlighted with asterisks (*).

In summary, these results suggest that MagNP-OH fulfill the biosafety and biocompatibility requirements for future clinical use. Incorporation of these MNPs in fibrin-agarose biomaterials allows the generation of novel biomaterials with improved biomechanical properties with guarantees of biosafety and biocompatibility demonstrated at the morphological, structural and functional levels. As an alternative route of delivery, tissue-like biomaterials allow an efficient control of the MNPs biodistribution *in vivo*. Biodistribution analysis demonstrated that our strategy supports the local use of the MagNP-OH, which were mostly confined to the implantation area. In addition, tissue-like biomaterials based on fibrin-agarose combined with MagNP-OH allows easy handling and straightforward surgical implant of these nanoparticles, and facilitates local *in vivo* encapsulation of MagNP-OH as compared to injected MagNP-OH. In addition, the methodology described in the present manuscript also allowed the generation of novel biomaterials with a definite structural alignment using magnetic fields during gelation of the biomaterial. This could be advantageous for reproduction and treatment of human tissues requiring a specific 3D structural organization such as the human cornea [52], tendon [53] and cartilage [54] and also other tissues with an anisotropic behavior such as the human skin, nerve and oral mucosa and palate [55]. However, future clinical trials should demonstrate the usefulness of these tissue-like products.

4. Conflicts of interest

The authors declare that they have no known competing financial interests or personal relationships that could have appeared to influence the work reported in this paper.

5. Author contributions

MTLL performed magnetic particles characterization. IAR and MA developed in vitro analyses of biocompatibility. ABBE, JDGD and MTLL performed the mechanical properties. FC, IAR, ABBE and VC performed the surgery of animals. FC, IAR and VC performed and analysed the magnetic resonance imaging. IAR, ABBE and VC developed and analysed the data of haematological and biochemical studies. FC, IAR, ABBE and VC developed histological and histochemical studies. IAR and VC analysed data of histology. RC, IAR and VC performed the ultrastructural study. MTLL, ABBE and PK, performed magnetometry. FC and MA statistical analyses. IAR, FC, VC, MA and MTLL performed the experimental design and wrote this work.

6. Acknowledgements

This study was supported by the following grants:

- Grants FIS-PI17/0391 and FIS-PI17/0393 from Instituto de Salud Carlos III - ISCIII (Plan Nacional de Investigación Científica, Desarrollo e Innovación Tecnológica I+D+i from the Spanish Ministerio de Asuntos Económicos y Transformación Digital), co-financed by ERDF-FEDER, European Union.
- Award number AC17/00013 (NanoGSkin) by ISCIII thorough AES 2017 and within the EuroNanoMed framework.
- Grant FIS2017-85954-R funded by Ministerio de Economía, Industria y Competitividad, MINECO, and Agencia Estatal de Investigación, AEI, Spain, cofunded by Fondo Europeo de Desarrollo Regional, FEDER, European Union.
- Grants CS PI-0257-2017 and CSyF PE-0395-2019 from Consejería de Salud y Familias, Junta de Andalucía, Spain.
- Grant nº Res SECYT 411/18 from SECYT (Secretary of Science and Technology of National University of Córdoba, Argentina)
- Project Future Investments UCA JEDI, No. ANR-15-IDEX-01, project "RheoGel" by the French "Agence Nationale de la Recherche".

References

[1] A. Cervadoro, C. Giverso, R. Pande, S. Sarangi, L. Preziosi, J. Wosik, A. Brazdeikis, P. Decuzzi, PLoS One, 8 (2013) e57332.
[2] K. Andreas, R. Georgieva, M. Ladwig, S. Mueller, M. Notter, M. Sittinger, J. Ringe, Biomaterials, 33 (2012) 4515-4525.
[3] X.W. Chen, Q.X. Mao, J.W. Liu, J.H. Wang, Talanta, 100 (2012) 107-112.
[4] J. Qin, K. Li, C. Peng, X. Li, J. Lin, K. Ye, X. Yang, Q. Xie, Z. Shen, Y. Jin, M. Jiang, G. Zhang, X. Lu, Biomaterials, 34 (2013) 4914-4925.
[5] G.Y. Lee, W.P. Qian, L. Wang, Y.A. Wang, C.A. Staley, M. Satpathy, S. Nie, H. Mao, L. Yang, ACS Nano, 7 (2013) 2078-2089.
[6] S. Jiang, A.A. Eltoukhy, K.T. Love, R. Langer, D.G. Anderson, Nano Lett, 13 (2013) 1059-1064.
[7] K. Niemirowicz, K.H. Markiewicz, A.Z. Wilczewska, H. Car, Adv Med Sci, 57 (2012) 196-207.
[8] M.J. Alonso, S. Cohen, T.G. Park, R.K. Gupta, G.R. Siber, R. Langer, Pharm Res, 10 (1993) 945-953.
[9] S. Behrens, Nanoscale, 3 (2011) 877-892.
[10] L.H. Reddy, J.L. Arias, J. Nicolas, P. Couvreur, Chem Rev, 112 (2012) 5818-5878.
[11] M.T. Lopez-Lopez, G. Scionti, A.C. Oliveira, J.D. Duran, A. Campos, M. Alaminos, I.A. Rodriguez, PLoS One, 10 (2015) e0133878.
[12] L. Rodriguez-Arco, I.A. Rodriguez, V. Carriel, A.B. Bonhome-Espinosa, F. Campos, P. Kuzhir, J.D. Duran, M.T. Lopez-Lopez, Nanoscale, 8 (2016) 8138-8150.
[13] R. De Santis, A. Russo, A. Gloria, U. D'Amora, T. Russo, S. Panseri, M. Sandri, A. Tampieri, M. Marcacci, V.A. Dediu, C.J. Wilde, L. Ambrosio, J Biomed Nanotechnol, 11 (2015) 1236-1246.
[14] C. Chouly, D. Pouliquen, I. Lucet, J.J. Jeune, P. Jallet, J Microencapsul, 13 (1996) 245-255.

[15] X.B. Zeng, H. Hu, L.Q. Xie, F. Lan, W. Jiang, Y. Wu, Z.W. Gu, Int J Nanomedicine, 7 (2012) 3365-3378.
[16] N. Bock, A. Riminucci, C. Dionigi, A. Russo, A. Tampieri, E. Landi, V.A. Goranov, M. Marcacci, V. Dediu, Acta Biomater, 6 (2010) 786-796.
[17] A.B. Bonhome-Espinosa, F. Campos, I.A. Rodriguez, V. Carriel, J.A. Marins, A. Zubarev, J.D.G. Duran, M.T. Lopez-Lopez, Soft Matter, 13 (2017) 2928-2941.
[18] J.S. Kim, T.J. Yoon, K.N. Yu, B.G. Kim, S.J. Park, H.W. Kim, K.H. Lee, S.B. Park, J.K. Lee, M.H. Cho, Toxicol Sci, 89 (2006) 338-347.
[19] M. Alaminos, M. Del Carmen Sanchez-Quevedo, J.I. Munoz-Avila, D. Serrano, S. Medialdea, I. Carreras, A. Campos, Investigative ophthalmology & visual science, 47 (2006) 3311-3317.
[20] F. Campos, A.B. Bonhome-Espinosa, G. Vizcaino, I.A. Rodriguez, D. Duran-Herrera, M.T. Lopez-Lopez, I. Sanchez-Montesinos, M. Alaminos, M.C. Sanchez-Quevedo, V. Carriel, Biomedical materials, 13 (2018) 025021.
[21] V. Carriel, I. Garzon, J.M. Jimenez, A.C. Oliveira, S. Arias-Santiago, A. Campos, M.C. Sanchez-Quevedo, M. Alaminos, Cells, tissues, organs, 196 (2012) 1-12.
[22] V. Carriel, G. Scionti, F. Campos, O. Roda, B. Castro, M. Cornelissen, I. Garzon, M. Alaminos, Journal of tissue engineering and regenerative medicine, 11 (2017) 1412-1426.
[23] I.A. Rodriguez, M.T. Lopez-Lopez, A.C. Oliveira, M.C. Sanchez-Quevedo, A. Campos, M. Alaminos, J.D. Duran, Journal of tissue engineering and regenerative medicine, 6 (2012) 636-644.
[24] M.C. Sanchez-Quevedo, M. Alaminos, L.M. Capitan, G. Moreu, I. Garzon, P.V. Crespo, A. Campos, Histol Histopathol, 22 (2007) 631-640.
[25] J. Chato-Astrain, F. Campos, O. Roda, E. Miralles, D. Durand-Herrera, J.A. Saez-Moreno, S. Garcia-Garcia, M. Alaminos, A. Campos, V. Carriel, Frontiers in cellular neuroscience, 12 (2018) 501.
[26] V. Carriel, G. Vizcaino-Lopez, J. Chato-Astrain, D. Durand-Herrera, M. Alaminos, A. Campos, I. Sanchez-Montesinos, F. Campos, Exp Eye Res, 186 (2019) 107717.
[27] M. Lopez-Lopez, I. Rodriguez, L. Rodriguez-Arco, V. Carriel, A. Bonhome-Espinosa, F. Campos, A. Zubarev, J. Duran, Journal of Magnetism and Magnetic Materials, 431 (2017) 110-114.
[28] F. Campos, A.B. Bonhome-Espinosa, L. Garcia-Martinez, J.D. Duran, M.T. Lopez-Lopez, M. Alaminos, M.C. Sanchez-Quevedo, V. Carriel, Biomedical materials, 11 (2016) 055004.
[29] I.A. Rodriguez, C.A. Ferrara, F. Campos-Sanchez, M. Alaminos, J.U. Echevarria, A. Campos, J Adhes Dent, 15 (2013) 541-546.
[30] V. Carriel, I. Garzon, M. Alaminos, M. Cornelissen, Neural Regen Res, 9 (2014) 1657-1660.
[31] M.A. Rodriguez, M.T. Lopez-Lopez, J.D. Duran, M. Alaminos, A. Campos, I.A. Rodriguez, Cryobiology, 67 (2013) 355-362.
[32] J. Chato-Astrain, C. Philips, F. Campos, D. Durand-Herrera, O. García-García, A. Roosens, M. Alaminos, A. Campos, V. Carriel, Journal of tissue engineering and regenerative medicine, (2020).
[33] V. Carriel, J. Garrido-Gomez, P. Hernandez-Cortes, I. Garzon, S. Garcia-Garcia, J.A. Saez-Moreno, M. Del Carmen Sanchez-Quevedo, A. Campos, M. Alaminos, J Neural Eng, 10 (2013) 026022.
[34] A. Gloria, T. Russo, U. D'Amora, S. Zeppetelli, T. D'Alessandro, M. Sandri, M. Banobre-Lopez, Y. Pineiro-Redondo, M. Uhlarz, A. Tampieri, J. Rivas, T. Herrmannsdorfer, V.A. Dediu, L. Ambrosio, R. De Santis, J R Soc Interface, 10 (2013) 20120833.
[35] A. Tampieri, T. D'Alessandro, M. Sandri, S. Sprio, E. Landi, L. Bertinetti, S. Panseri, G. Pepponi, J. Goettlicher, M. Banobre-Lopez, J. Rivas, Acta Biomater, 8 (2012) 843-851.

[36] A. Tampieri, E. Landi, F. Valentini, M. Sandri, T. D'Alessandro, V. Dediu, M. Marcacci, Nanotechnology, 22 (2011) 015104.
[37] M.T. Lopez-Lopez, A. Gomez-Ramirez, L. Rodriguez-Arco, J.D. Duran, L. Iskakova, A. Zubarev, Langmuir, 28 (2012) 6232-6245.
[38] A.K. Gupta, M. Gupta, Biomaterials, 26 (2005) 3995-4021.
[39] R. Weissleder, D.D. Stark, B.L. Engelstad, B.R. Bacon, C.C. Compton, D.L. White, P. Jacobs, J. Lewis, AJR. American journal of roentgenology, 152 (1989) 167-173.
[40] C. Song, X. Meng, Y. Liu, A. Shen, C. Shao, K. Wang, H. Cheng, X. Fang, P. Wang, W. Bu, Biomaterials, 230 (2020) 119631.
[41] L. Rico-Sanchez, I. Garzon, M. Gonzalez-Andrades, A. Ruiz-Garcia, M. Punzano, A. Lizana-Moreno, J.I. Munoz-Avila, M.D.C. Sanchez-Quevedo, J. Martinez-Atienza, L. Lopez-Navas, R. Sanchez-Pernaute, R.I. Oruezabal, S. Medialdea, M.D.C. Gonzalez-Gallardo, G. Carmona, S. Sanbonmatsu-Gamez, M. Perez, P. Jimenez, N. Cuende, A. Campos, M. Alaminos, Journal of tissue engineering and regenerative medicine, 13 (2019) 2142-2154.
[42] E.A. Neuwelt, C.G. Varallyay, S. Manninger, D. Solymosi, M. Haluska, M.A. Hunt, G. Nesbit, A. Stevens, M. Jerosch-Herold, P.M. Jacobs, J.M. Hoffman, Neurosurgery, 60 (2007) 601-611; discussion 611-602.
[43] M. Wankhede, A. Bouras, M. Kaluzova, C.G. Hadjipanayis, Expert Rev Clin Pharmacol, 5 (2012) 173-186.
[44] P. Lakhani, K.K. Dwivedi, N. Kumar, J Mech Behav Biomed Mater, 104 (2020) 103693.
[45] C. Gila-Vilchez, M.C. Manas-Torres, R. Contreras-Montoya, M. Alaminos, J.D.G. Duran, L.A. de Cienfuegos, M.T. Lopez-Lopez, Philos Trans A Math Phys Eng Sci, 377 (2019) 20180217.
[46] E. Teeman, C. Shasha, J.E. Evans, K.M. Krishnan, Nanoscale, 11 (2019) 7771-7780.
[47] A.S. Zhang, C.A. Enns, Hematology. American Society of Hematology. Education Program, (2009) 207-214.
[48] N. Dasgupta, S. Ranjan, C. Ramalingam, M. Gandhi, 3 Biotech, 9 (2019) 125.
[49] H.C. Janssen, N. Angrisani, S. Kalies, F. Hansmann, M. Kietzmann, D.P. Warwas, P. Behrens, J. Reifenrath, J Nanobiotechnology, 18 (2020) 14.
[50] L. Johnson, S.E. Pinder, M. Douek, Histopathology, 62 (2013) 481-486.
[51] I. Kampfmann, N. Bauer, S. Johannes, A. Moritz, Veterinary clinical pathology, 41 (2012) 228-234.
[52] A. Isaacson, S. Swioklo, C.J. Connon, Exp Eye Res, 173 (2018) 188-193.
[53] A. Sensini, C. Gualandi, A. Zucchelli, L.A. Boyle, A.P. Kao, G.C. Reilly, G. Tozzi, L. Cristofolini, M.L. Focarete, Sci Rep, 8 (2018) 17167.
[54] J.P. Wu, T.B. Kirk, M.H. Zheng, J Orthop Surg Res, 3 (2008) 29.
[55] P. Liu, J.Y. Zhu, B. Tang, Z.C. Hu, J Microsc, 270 (2018) 170-175.

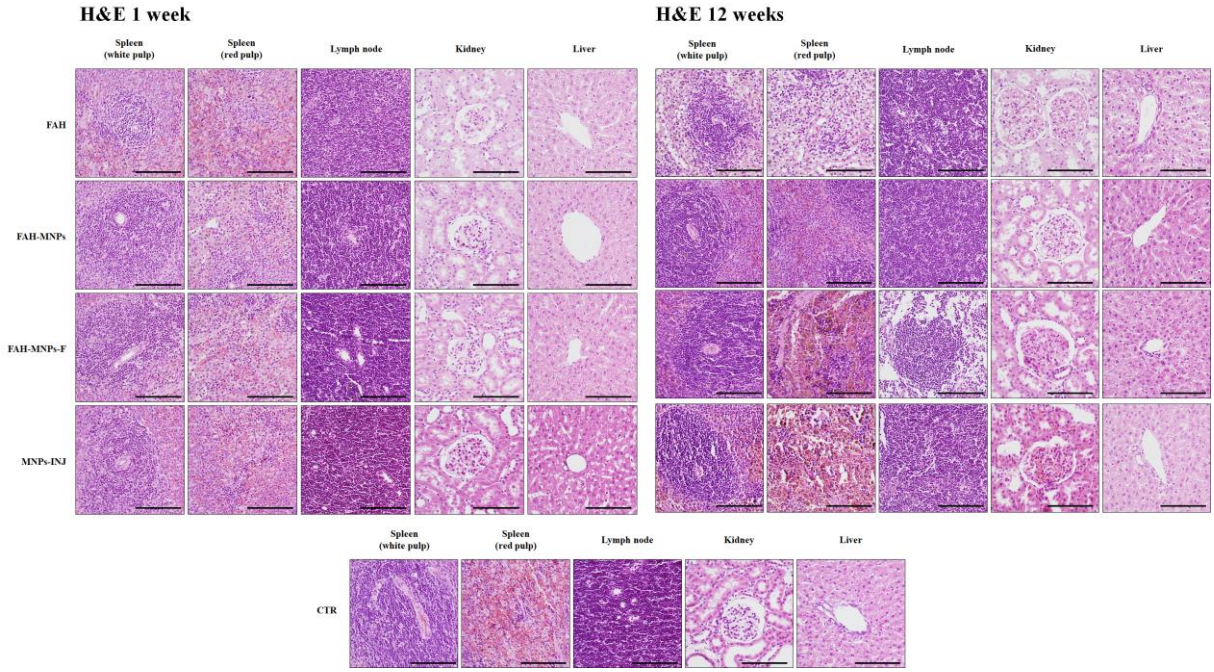

Supplementary Figure S1. Histological analysis of four major distal organs using Hematoxylin and Eosin staining (H&E). FAH: fibrin-agarose hydrogels; FAH-MNPs: FAH containing MagNP-OH; FAH-MNPs-F: FAH containing MagNP-OH subjected to magnetic field during gelation; MNPs-INJ: MNPs injected subcutaneously; CTR: control animals. Scale bar 100 µm

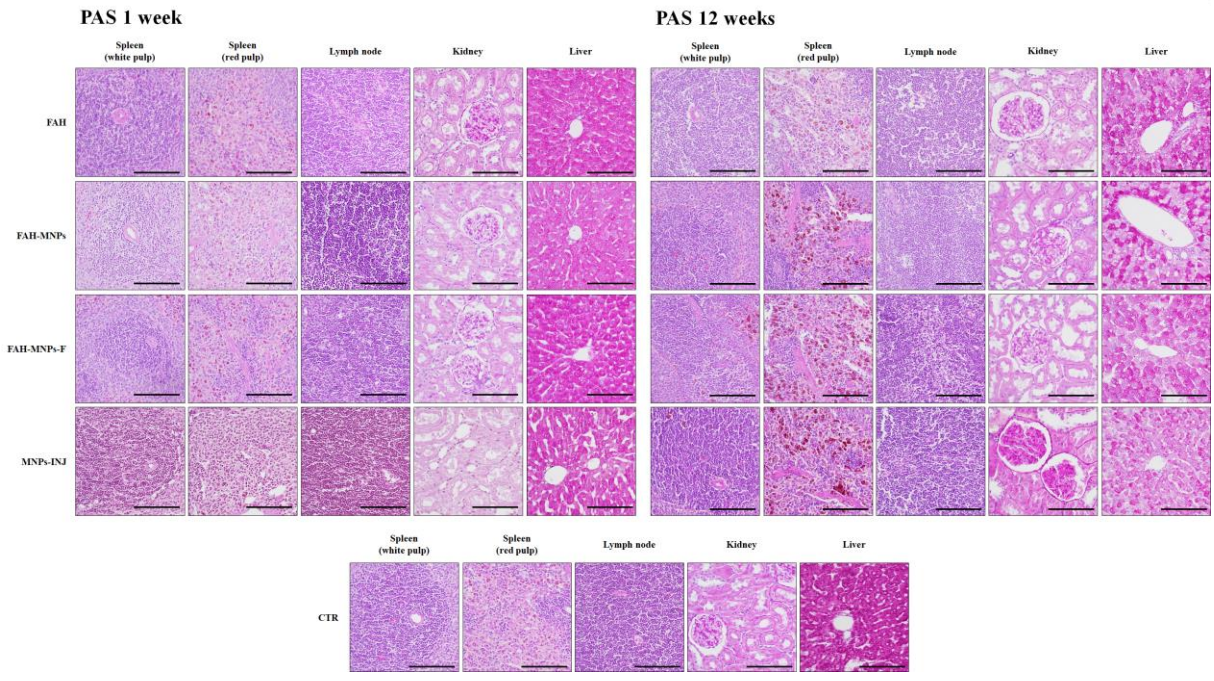

Supplementary Figure S2. Histochemical analysis of four major distal organs using the PAS method. FAH: fibrin-agarose hydrogels; FAH-MNPs: FAH containing MagNP-OH; FAH-MNPs-F: FAH containing MagNP-OH subjected to magnetic field during gelation; MNPs-INJ: MNPs injected subcutaneously; CTR: control animals. Scale bar 100 µm